JEE Journal of Ecological Engineering

Journal of Ecological Engineering, 2026, 27(5), 273–290
https://doi.org/10.12911/22998993/216102
ISSN 2299–8993, License CC-BY 4.0

Received: 2025.11.25
Accepted: 2025.12.26
Published: 2026.04.01

Flood risk assessment using HEC-RAS model and GIS for the Indus River, Pakistan

Saeed Ur Rehman Aziz[1*], Muhammad Arshad[1], Muhammad Adnan Shahid[1,2], Ejaz Ahmad Waraich[3], Venkatesh Merwade[4]

[1] Department of Irrigation and Drainage, University of Agriculture, Faisalabad 38000, Pakistan
[2] Agricultural Remote Sensing Lab (ARSL), National Center of GIS and Space Applications (NCGSA), Faisalabad 38000, Pakistan
[3] Department of Agronomy, University of Agriculture, Faisalabad 38000, Pakistan
[4] School of Civil Engineering, Purdue University, 550 Stadium Mall Drive, West Lafayette, IN 47907, USA
* Corresponding author's e-mail: engr.saeedaziz@gmail.com

ABSTRACT

Floods are among the most destructive natural hazards globally, causing extensive socioeconomic losses. The Indus River Basin, one of the world's largest, has experienced recurrent catastrophic floods; however, the absence of effective early warning systems continues to hinder timely disaster response. This study addresses this gap by analyzing extreme flood hazards along the 434-km Chashma–Kot Mithon reach using a one-dimensional HEC-RAS v6.3.0 model integrated with GIS, subdivided into Chashma–Taunsa and Taunsa–Kot Mithon sections. Annual peak flows from 2005 to 2022 were evaluated using the Generalized Extreme Value (GEV) distribution, selected through Kolmogorov–Smirnov and Anderson–Darling tests, to estimate discharges for multiple return periods. The Copernicus GLO-30 digital elevation model (30 m resolution) was refined in the HEC-RAS Mapper by incorporating control structures and bathymetric data to enhance the hydraulic accuracy of the model terrain. Calibration with the 2010 flood and validation with the 2006 flood demonstrated strong performance using differentiated Manning's n values (channel: 0.027; right bank: 0.055; left bank: 0.040), achieving NSE = 0.92–0.95, R^2 = 0.91–0.95, and RSR = 0.28–0.20. The 200-year scenario produced peak flows of 31,728 m^3/s at Chashma and 28,723 m^3/s at Taunsa, increasing inundation by 20.87% and 40.60%, respectively, compared to 2010. MODIS-based validation indicated acceptable accuracy, with overestimations of 8.86% and 4.87%, respectively. Hydrodynamic analysis revealed peak depths of 17 m and velocities of 4 m/s. District-scale assessment showed 10–11% inundation growth in Layyah and Muzaffargarh, whereas union council maps delineated high-risk and safe zones. These findings underscore the potential of HEC-RAS and GIS for proactive flood-risk management in the Indus Basin.

Keywords: Indus River, flood risk assessment, HEC-RAS, GIS, hydraulic modeling.

INTRODUCTION

Rivers are critical freshwater sources that support ecological integrity and human development and influence agriculture, settlement patterns, and economic systems (Martin, 2023). However, they also pose significant flood risks, with floods ranking among the most destructive natural hazards (Seyedeh et al., 2008; Younas et al., 2024). Despite progress in forecasting and hydraulic modeling the impact of floods remains severe, particularly in hydroclimatically variable regions such as Pakistan (Cea and Costabile, 2022; Tariq et al., 2021). Climate change, urbanization, population growth, and land use changes have intensified flood frequency and magnitude, underscoring the urgent need for predictive modeling and risk assessment to enhance resilience and disaster preparedness (Khan et al., 2024; Rizwan et al., 2023; Schürings et al., 2022).

Pakistan's dependence on the Indus River system makes it highly susceptible to recurrent flooding. As the country's primary water source and irrigation backbone, the Indus River poses seasonal flood risks driven by monsoon rains and snowmelt (Rizwan et al., 2023). The 2010

floods exemplified this vulnerability, displacing 20 million people, inundating 17 million acres of farmland, and destroying 1.8 million homes, among the costliest floods globally (CNN, 2010; Khosa, 2014; WB, 2010). Recovery efforts totaled $6.8 billion, while overall damages were estimated between $9.7 and $10 billion (FFC, 2010; Floods, 2010).

Embankment failures along the Taunsa reach intensified flooding in low-lying agricultural districts, such as Layyah and Muzaffargarh. Excessive monsoon rainfall, tributary inflows, and hill torrents overwhelmed the Chashma and Taunsa barrages, breaching their embankments (Gull et al., 2020; Syvitski and Brakenridge, 2013). The rainfall extremes of 468 mm in Risalpur and 384 mm in Cherat over four days highlighted the event's severity (Hashmi et al., 2012). The disaster was exacerbated by weak embankments, poor drainage, and unregulated settlements.

Integrated flood hazard mapping is essential, particularly when hydrodynamic modeling is combined with socio-economic variables considerations (Thaivalappil Sukumaran and Birkinshaw, 2024). Spatially explicit impact assessments rely on hydrological and hydraulic models to simulate flood extent and forecast its impacts (Afzal et al., 2022). Among the available tools, Hydrologic Engineering Center-River Analysis System (HEC-RAS) has proven effective in data-scarce environments by efficiently leveraging geographic data (Cook and Merwade, 2009). The model performs one-dimensional hydraulic simulations using cross-sections, boundary conditions, and Manning's roughness coefficients (Suro et al., 2024). Enhancements in GIS and remote sensing technologies support flood control by refining flood depth and flow estimations, and improving spatial attenuation analysis (Abdrabo, 2023; Akhtar, 2023; Wang and Xie, 2018).

HEC-RAS has demonstrated versatility and reliability in floodplain mapping and risk assessment across diverse hydrological contexts, both nationally and internationally. Its applicability has been demonstrated in studies by Manina et al. (2020), Indrawati et al. (2019), and Gumindoga et al. (2024). In urban flood modeling, Velychko and Dupliak (2024) highlighted its potential, while Peker et al. (2024) showed enhanced flood scenario simulation and risk mapping in the Göksu River Basin through integration of HEC-RAS, HEC-HMS, and GIS.

HEC-RAS has been extensively applied in Pakistan for riverine flood evaluations. Ullah et al. (2024) demonstrated its utility for the Swat River, highlighting the role of high-resolution digital elevation models (DEMs) in addressing complex mountainous terrain Khattak et al. (2016), Khalil and Khan (2017), and Salman et al. (2021) applied HEC-RAS–GIS floodplain mapping to evaluate flow dynamics and delineate floodplains along the Kabul River, Indus River, and Narai Drain, respectively. Afzal et al. (2022) integrated satellite imagery with HEC-RAS to support flood forecasting and early warning systems across the Indus Basin. Ijaz et al. (2019) emphasized DEM precision in hydrodynamic modeling, while Ahmad et al. (2022) enhanced forecasting accuracy by combining remote sensing and machine learning with HEC-RAS and GIS.

Despite the advancements in flood modeling, significant research gaps persist. The existing literature remains largely confined to localized contexts and short-duration flood events, often overlooking longer-return-period floods in highly vulnerable districts such as Layyah and Muzaffargarh (Khan et al., 2017). Given projections that climate change will intensify hydrological extremes across South Asia (Cui et al., 2023; Mujumdar et al., 2020), the need for comprehensive modeling and long-term analysis is critical.

This study evaluated a one-dimensional HEC-RAS model, calibrated with high-resolution DEM and bathymetric data, to simulate historical and extreme floods along the Chashma–Taunsa–Kot Mithon reach. This study will estimate the peak flood discharges with different return periods using the best-fit probability distributions, and then estimate flood extents, depths, and velocities for flood magnitudes of different return periods, compare the simulated 2010 inundation with MODIS observations, and identify highly vulnerable areas in Layyah and Muzaffargarh under the 200-year scenario to inform flood-risk planning. They aid sustainable land-use planning and contribute to detailed flood maps of depth, velocity, and extent. These outputs offer essential guidance for decision-makers in developing climate-resilient flood control and mitigation strategies, particularly for high-magnitude flash flood events.

MATERIALS AND METHODS

Study area and background

The Indus Basin spans over 1,165,000 km² and is distributed across China (10.7%), Afghanistan (6.7%), India (26.6%), and predominantly Pakistan (56%) (Afzal et al., 2022). Originating from Lake Mansarovar on the Tibetan Plateau, the Indus River flows through Kashmir and Pakistan before discharging into the Arabian Sea. The Upper Indus Basin, located near 32.48° N and 67.33° E, encompasses the Karakoram, Hindu Kush, and Himalayan ranges, containing approximately 11,000 glaciers over 22,000 km², making it one of the largest temperate glaciated regions outside the polar zones (Bajracharya and Shrestha, 2011; Lutz et al., 2016). Elevations range from 200 to 8500 m, with an average of 3750 m. The basin is a critical freshwater source for Pakistan, supporting agriculture, hydropower, and domestic water supplies (Afzal et al., 2022).

The 2010 flood event was notably severe, exacerbated by hill torrents from Sangar and Vehowa hazards (Syvitski and Brakenridge, 2013; Tariq et al., 2021). The Layyah and Muzaffargarh districts, characterized by flat, densely cultivated floodplains, face increasing flood risks due to rapid urbanization, agricultural expansion, neglected floodplain settlements, and embankment failures (Gull et al., 2020). Enhancing flood risk management and resilience is essential for sustainable development and disaster mitigation in these areas.

The hydrological records of the Indus River show significant variability. The peak discharges in 2010 reached 27,108 m³/s at Taunsa and 22,614 m³/s at Chashma, while the minimum flows in 2004 were 6061 m³/s and 5164 m³/s, respectively, confirming the extremity of the 2010 flood (PMIU, 2022). Figure 1 shows the study area.

The Chashma–Kot Mithon (CK) reach of the Indus River spans approximately 434 km and is divided into two reaches: Chashma–Taunsa (CT; 252 km) and Taunsa–Kot Mithon (TK; 182 km) (Figure 2). Gauge stations are available at Chashma and Taunsa, Pakistan. A hydraulic model was developed and calibrated for the CT reach, and the validated parameters were applied to the TK reach, which lacked direct gauge data.

Overview of the geographic information systems

Geographic information systems (GIS) provide an integrated framework for the acquisition, management, analysis, and visualization of spatial data, enabling effective examination of environmental and flood-related processes. By combining datasets such as topography, hydrology, land use, infrastructure, rainfall, and satellite imagery, GIS supports accurate representation of terrain characteristics and surface-water dynamics, making it an essential tool for flood risk assessment and floodplain mapping.

GIS also facilitates hazard mapping, vulnerability assessment, and informed decision-making by integrating hydrodynamic model outputs—such as flood extent, depth, and velocity—with real-world geographic features. Coupling GIS with hydrologic and hydraulic models, particularly HEC-RAS, significantly enhances the accuracy and spatial resolution of flood inundation mapping (Kim et al., 2020; Korjenić et al., 2021). The incorporation of remote sensing data, including MODIS and Sentinel imagery, further strengthens model validation and flood monitoring by enabling comparisons between simulated and observed inundation patterns (George et al., 2022).

Beyond methodological advancements, GIS-based flood mapping functions as a critical decision-support tool by identifying flood-prone areas, assessing impacts on infrastructure and communities, and informing evidence-based land-use planning and disaster risk-reduction strategies (Ibrahim et al., 2024; Prasad et al., 2022). The continued integration of GIS, remote sensing, and hydrodynamic modeling remains central to the development of proactive and effective flood mitigation strategies (Gomma, 2021; Yonehara and Kawasaki, 2020)

Description of the hydrological model

HEC-RAS, developed by the U.S. Army Corps of Engineers is one of the most popular hydraulic modeling frameworks for river flow, flood risk, and hazard mapping (CEIWR-HEC, 2023). HEC-RAS in its one-dimensional (1D) version solves the Saint-Venant equations and computes vertically one-dimensional profiles along the river channels. The model incorporates energy and momentum equations, enabling an accurate representation of both rapidly and gradually varying flows.

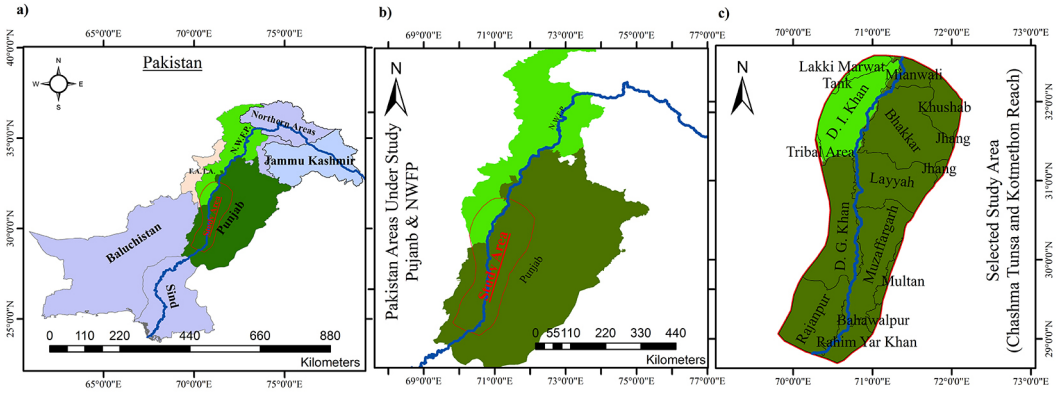

Figure 1. Study area: (a) Pakistan, (b) Punjab and North-West Frontier Province (NWFP) areas under study, (c) Districts of Punjab and NWFP along the Chashma–Kot Mithan study reach.

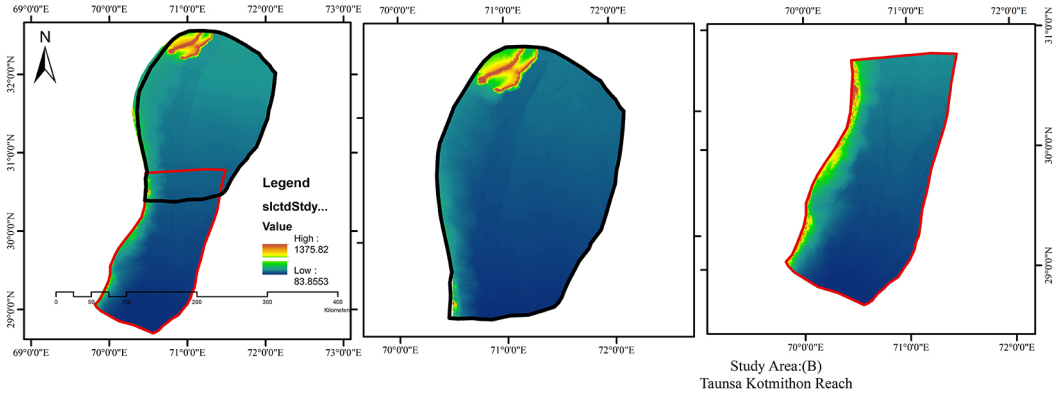

Figure 2. Copernicus digital elevation model (GLO-30 DEM): (a) Subdivision of the study area into two reaches, (b) Chashma–Taunsa reach (CT), (c) Taunsa-Kot Mithon Reach

Figure 3 depicts all the components of the energy equation. For gradually varied flows, the water surface elevations were determined using the 1D steady-flow energy equation solved iteratively between successive cross-sections using the standard step method (Brunner, 2010).

The governing energy equation is given by Equation 1.

$$Z_1 + Y_1 + \frac{\alpha_1 V_1^2}{2g} = Z_2 + \\ +Y_2 + \frac{\alpha_2 V_2^2}{2g} + h_e \quad (1)$$

where: Z_1 *and* Z_2 – elevations of the main channel, Y_1 *and* Y_2 – flow depths at the respective cross-sections, α_1 *and* α_2 – velocity weighting coefficients, V_1 *and* V_2 – average velocities, g – gravitational acceleration, h_e – energy loss between the upstream and downstream cross-sections.

Calibration in 1D HEC-RAS models is typically easier than that in 2D models. The integration of GIS with model outputs improved spatial visualization, facilitating accurate floodplain mapping and disaster preparedness. Nevertheless, the oversimplified assumptions of the 1D framework limit its potential to analyze floodplain dynamics laterally and in complex geomorphological situations, which can hinder the accuracy of overbank inundation models (Teng et al., 2017). Despite these drawbacks, the 1D HEC-RAS model is a practical and well-developed model used worldwide for large river systems, primarily because of its combined reliability and efficiency as a predictive tool (Horritt and Bates, 2002).

Data collection and flood frequency analysis

Annual peak and daily discharge data for 2005–2022 were acquired from the Punjab Irrigation Department (PID) and the Program Monitoring and Implementation Unit (PMIU). Six-hourly discharge records from the 2010 flood and daily data from the 2006 flood were used for trend

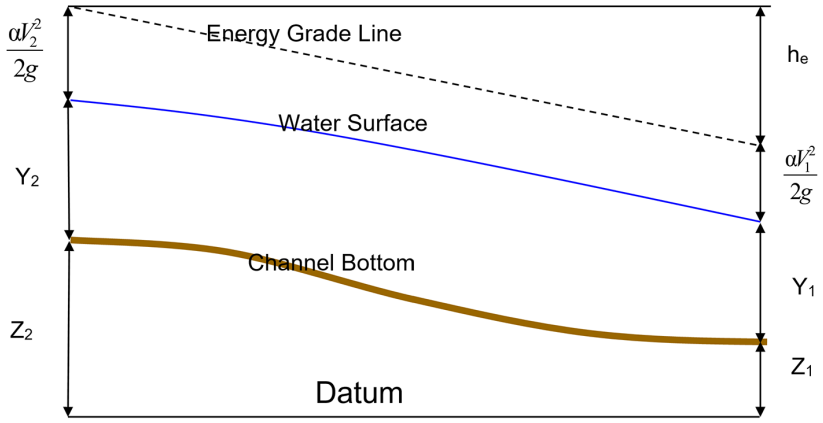

Figure 3. Components of the energy equation (CEIWR-HEC, 2022)

analysis, model calibration, and validation. The 2010 flood was selected as the calibration event because of the availability of detailed hydrographic and inundation data, whereas the 2006 flood was used for validation purposes.

Flood frequency analysis was conducted using EasyFit software, applying multiple probability distributions, including Normal, Lognormal, Gumbel, Log-Pearson Type III (LP3), and Generalized Extreme Value (GEV), to annual peak flow data at Chashma. Based on goodness-of-fit evaluations using the Kolmogorov–Smirnov and Anderson–Darling tests, the GEV and Gumbel distributions provided the best fit. Design discharges corresponding to return periods of 5, 25, 50, 100, and 200 years were derived using the 2010 hydrograph as the reference template for constructing design flood scenarios.

Statistical evaluation of HEC-RAS model performance

Hydraulic models, such as HEC-RAS, require statistical measures to determine how well simulated hydrographs correspond with observed hydrographs to evaluate calibration and validation. According to the U.S. Army Corps of Engineers, model accuracy and consistency were measured with respect to four metrics that are among the most commonly used in the field: Nash-Sutcliffe Efficiency (NSE), ratio of the root mean square error to standard deviation (RSR), percent bias (PBIAS), and coefficient of determination (R^2) (CEIWR-HEC, 2023). Collectively, these measures provide the most useful and complementary insights regarding the alignment of the simulated and observed datasets pertaining to discharge and water surface elevations, which informs the reliability and predictive value of the hydrodynamic simulations.

Nash-Sutcliffe Efficiency

NSE evaluates model performance by comparing the residual variance of the simulated data to the variance of the observed data, indicating how closely the simulations align with the 1:1 line of agreement. The NSE values range from $-\infty$ to 1.0, where 1.0 denotes perfect correspondence and negative values indicate poor performance, which is worse than the observed mean. Its ability to capture both the temporal and magnitude aspects of flow makes the NSE one of the most widely used metrics in hydrology. The formulation of the NSE is presented in Equation 2.

$$NSE = 1 - \frac{\sum_{i=1}^{n}(Y_i^{obs} - Y_i^{sim})^2}{\sum_{i=1}^{n}(Y_i^{obs} - \bar{Y}_{obs})^2} \quad (2)$$

where: Y_i^{obs} – observed values, Y_i^{sim} – simulated values.

Root mean square error to standard deviation ratio

The root mean square error to standard deviation ratio is calculated by dividing the root mean square error (RMSE) by the standard deviation of the observed data, yielding a dimensionless metric suitable for cross-dataset and model comparisons. An RSR value of 0.0 indicates perfect agreement between the simulated and observed values, with lower values reflecting improved model performance by minimizing the residual variance. The RSR formulation is presented in Equation 3.

$$RSR = \frac{RMSE}{\sigma_{obs}} = \frac{\sqrt{\sum_{i=1}^{n}(Y_i^{obs} - Y_i^{sim})^2}}{\sqrt{\sum_{i=1}^{n}(Y_i^{obs} - \bar{Y}_{obs})^2}} \quad (3)$$

where: σ_{obs} – standard deviation, Y_i^{obs} – observed values, Y_i^{sim} – simulated values.

Percent bias

PBIAS quantifies the average tendency of simulated values to deviate from observed data, indicating model bias. A PBIAS of 0% reflects perfect agreement, negative values indicate underestimation, and positive values indicate overestimation. Although PBIAS can theoretically range from 0% to positive infinity, acceptable thresholds depend on the model type and study objectives. PBIAS is widely used to characterize systematic deviations and realistically represent discharge magnitudes and the water balance. The formulation is provided in Equation 4, as follows:

$$PBIAS = \frac{\sum_{i=1}^{n}(Y_i^{sim} - Y_i^{obs}) \times 100}{\sum_{i=1}^{n} Y_i^{obs}} \quad (4)$$

where: Y_i^{obs} – observed values, Y_i^{sim} – simulated values.

A PBIAS value close to 0% denotes optimal model performance, whereas negative or positive deviations reflect under and over-simulation, respectively.

Coefficient of determination

The coefficient of determination quantifies the correlation between the simulated and observed datasets, indicating how well the model explains the data variability. The R^2 values ranged from 0 to 1, with 1 representing a perfect fit. While R^2 provides insight into explanatory power, it is sensitive to outliers and may overlook any systematic bias. Therefore, it is best interpreted alongside other metrics, such as the NSE and RSR. The formulation of R^2 is presented in Equation 5.

$$R^2 = \left[\frac{\sum_{i=1}^{n}(Y_i^{obs} - \bar{Y}_{obs})}{\sqrt{\sum_{i=1}^{n}(Y_i^{obs} - \bar{Y}_{obs})^2}} \frac{(Y_i^{sim} - \bar{Y}_{sim})}{\sqrt{\sum_{i=1}^{n}(Y_i^{sim} - \bar{Y}_{sim})^2}}\right]^2 \quad (5)$$

where: Y_i^{obs} – observed value, $\bar{Y}_{obs}$ – mean of observed values, Y_i^{sim} – simulated value, $\bar{Y}_{sim}$ – mean of simulated values.

HEC-RAS model development and hydrodynamic simulations

The hydraulic geometry for the study area was derived from the Copernicus GLO-30 DEM (30 m resolution) (OpenTopography, 2023) and integrated with river geometry data. Bathymetric profiles, levees, and embankments were refined using the HEC-RAS RAS Mapper, and Google Earth imagery was employed to verify and adjust the placement of hydraulic structures, ensuring terrain accuracy. Terrain modifications were implemented using cross-section interpolation and vector terrain modification tools to maintain consistency with the inundation model. The riverbed geometry was generated by developing cross-sections (XS) along surveyed profiles from NESPAK (1999), and DEM-derived bathymetric data were

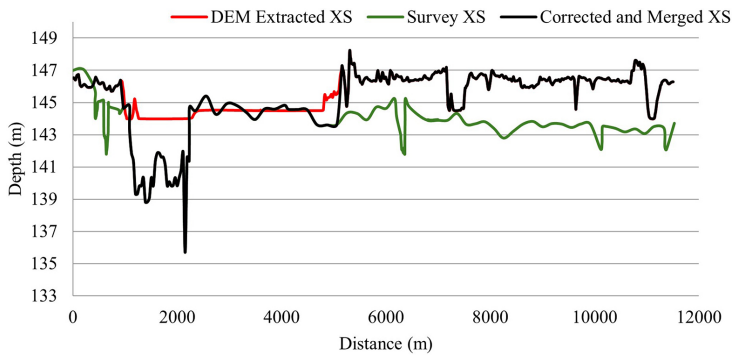

Figure 4. Copernicus digital elevation model (GLO-30 DEM) updated by merging surveyed cross-sections for river bathymetry

merged with these profiles to produce a continuous riverbed representation (Figure 4). A Triangulated Irregular Network (TIN) generated from the DEM served as the base terrain, with discrepancies resolved through satellite image comparison and manual correction in RAS Mapper (Figure 5).

Using the RAS Mapper, the river centerline, banks, flow paths, and cross-sectional views were digitized from upstream to downstream at intervals of 500–700 m and subsequently adjusted to closely align with the natural flow pathways. The geometry was exported to the geometric data editor, where the boundary conditions and Manning's roughness coefficients were configured (Figure 6). Different n values were assigned to the channel and floodplain separately to be able to spatially capture the flow resistance and facilitate better calibration.

Hydrodynamic simulations with HEC-RAS version 6.3.0 were performed using a 1D, unsteady flow model with 6 hourly hydrographs from the 2010 flood and 2006 daily discharge data at Chashma and Taunsa barrages (Figure 7–8). A normal depth condition was applied at the downstream end of the model. The shallow water equations were solved using the Eulerian–Lagrangian method (SWE-ELM) to ensure numerical stability and accuracy in long time steps.

Iterative adjustment of Manning's n values was performed for the Chashma–Taunsa reach to align the simulated water surface elevations with the observed data. Calibration and validation were assessed using statistical metrics – R^2, NSE, PBIAS, and RSE – all of which indicated satisfactory model performance. For the Taunsa–Kot Mithon reach, upstream-calibrated parameters were applied owing to the absence of downstream gauge data, assuming comparable hydraulic behavior.

Extreme flood simulation and GIS processing

The calibrated model was used to simulate a 200-year return period, representing extreme conditions relevant to flash flood events exacerbated by climate change. This design event allowed for the simulation of flood depth, velocity, and spatial extent within the study area. Flood hazard maps created from model outputs and analyzed in ArcGIS showed the inundation extent, depth, and velocity. For the Chashma–Kot Mithon reach, these maps hold significant value for flood risk assessment, informing infrastructure planning, and concentrating the identification of risk areas in the districts of Layyah and Muzaffargarh. The integration of the HEC-RAS results with GIS provided a new level of analytical foresight for the assessment of flood behavior and extent.

RESULTS AND DISCUSSIONS

Flood frequency analysis and hydrodynamic calibration

The Chashma–Kot Mithon reach encounters recurrent, high-magnitude floods, with the 2010 flood event being the greatest in recent decades. Flood magnitudes have changed over the years. According to the Federal Flood Commission (FFC) historical records and annual flood peak data (2005–2022), in 2006, the peak discharges recorded were 15,657 m^3/s at Chashma and 17,252 m^3/s at Taunsa, whereas during the 2010 flood event, the daily peak discharges were 27,108 m^3/s and 22,614 m^3/s, and the six-hourly

Figure 5. Copernicus digital elevation model (GLO-30 DEM) modifications: (a) without control structure, (b) Google Earth image of control structure, (c) regenerated structure

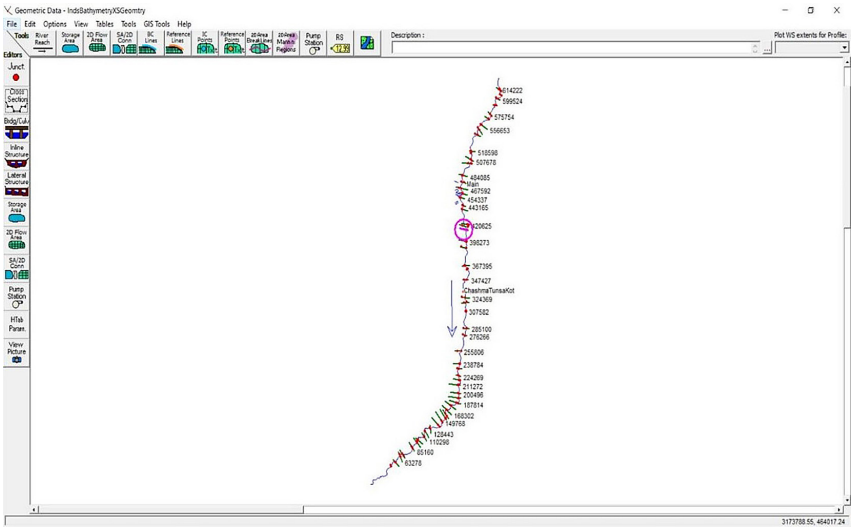

Figure 6. Geometric data window showing new study area geometry

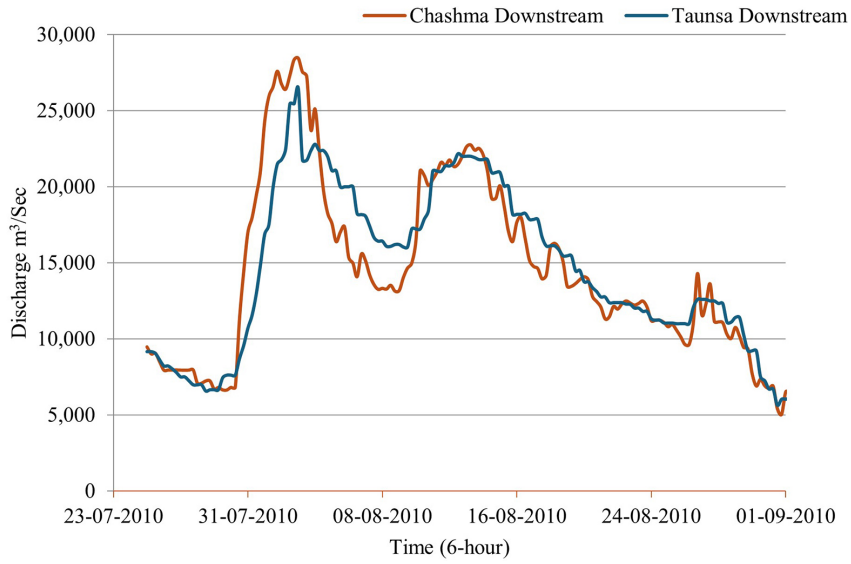

Figure 7. 2010 flood flow hydrographs at Chashma and Taunsa used as boundary conditions

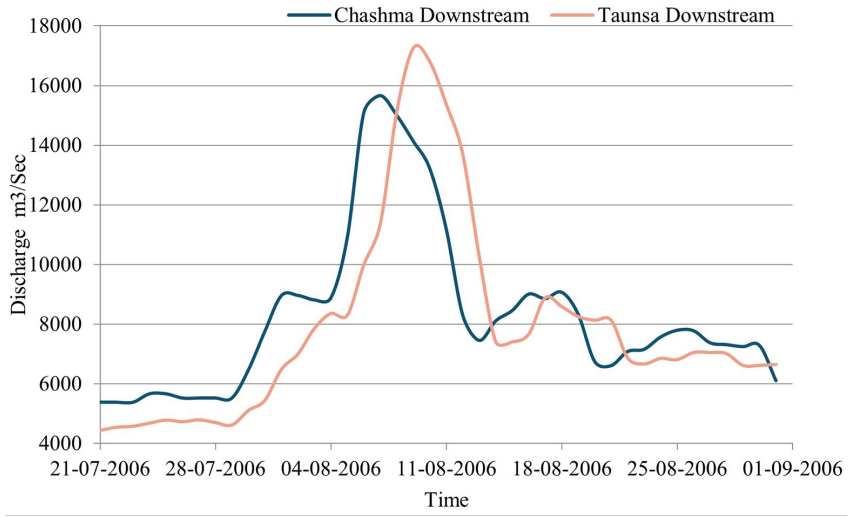

Figure 8. 2006 flood flow hydrographs at Chashma and Taunsa used as boundary conditions

discharges reached extreme values of 28,445 m³/s and 26,451 m³/s, respectively. The extreme values reached during the 2010 flood justify its selection as the flood event for hydraulic model calibration and validation.

For the period between 2005 and 2022, the annual maximum discharge series was utilized to conduct a flood frequency analysis to estimate the design flows for several return periods. The software EasyFit was used to analyze five different probability distributions: Normal, Log-Normal, Gumbel, Log-Pearson Type III, and GEV. Out of the the GEV, Log-Pearson Type III, and Gumbel distributions, GEV was selected as the "best" by the goodness of fit tests (Anderson-Darling and Kolmogorov-Smirnov). The GEV was chosen for its shape parameter flexibility and robustness in modeling extremes (Table 1) (Abbasnezhadi et al., 2020; Boucefiane and Meddi, 2022; Coles et al., 2001), whereas Log-normal 3P was poorly reliable owing to sample size and outlier sensitivity (Hosking and Wallis, 1997; Nguyen et al., 2017).

Peak discharges for return periods of 5 to 200 years were derived from the GEV (Table 2). At Chashma, the flow (Q) increased from 16,389 m³/s (5-year) to 31,728 m³/s (200-year), and at Taunsa, it increased from 14,998 m³/s to 28,723 m³/s. The corresponding reduced variance (K) values increased from 1.50 to 5.30. There was a clear, progressive increase in flood magnitude with longer return periods, reiterating the need for a hydrograph-based approach to assess flood risk and design hydraulic infrastructure. Figures 9 and 10 illustrate the hydrographs generated from the 2010 flood event for the different return periods.

Model calibration and validation

In accordance with U.S. Following the Army Corps of Engineers guidelines and Moriasi (2007), the HEC-RAS model was validated and calibrated using the NSE, PBIAS, RSR, R^2, and correlation coefficient (CEIWR-HEC, 2023; Moriasi et al., 2007). Brunner (2016) and Goodell (2014) suggested a normal-depth condition imposed at the downstream boundary (computed using Manning's equation) when the boundary is sufficiently far downstream to reduce backwater effects (Brunner, 2016; Goodell, 2014).

During calibration, strong agreement between the observed and simulated flow for the 2010 flood hydrograph resulted in NSE = 0.92, PBIAS = 2.07%, RSR = 0.28, R^2 = 0.91, and correlation coefficient = 0.95. Model validation with the 2006 flood NSE = 0.95, PBIAS = 1.13%, RSR = 0.20, R^2 = 0.95, and correlation coefficient = 0.97 also confirmed the robust calibration. Both datasets satisfied the performance benchmarks, confirming their strong predictive accuracy.

Table 1. Ranking of probability distributions after GOF statistical test using EasyFit

Distributions	Anderson Darling		Kolmogorov Smirnov	
	Statistics	Rank	Statistics	Rank
GEV	0.16859	1	0.09727	2
Lognormal 3P	0.17945	2	0.09169	1
Lognormal	0.29258	3	0.15999	4
Gumbel Max	0.34863	4	0.14256	3
Normal	0.83524	5	0.19396	6

Note: GOF – goodness-of-fit, GEV – generalized extreme value.

Table 2. Flood magnitudes for different return periods estimated using GEV

Probability distribution	Return period	Reduce variance K	Chashma Q m³/sec	Taunsa Q m³/sec
GEV	5	1.50	16389	14998
	25	3.20	23253	21139
	50	3.90	26095	23683
	100	4.60	28917	26207
	200	5.30	31728	28723

Note: GEV – generalized extreme value.

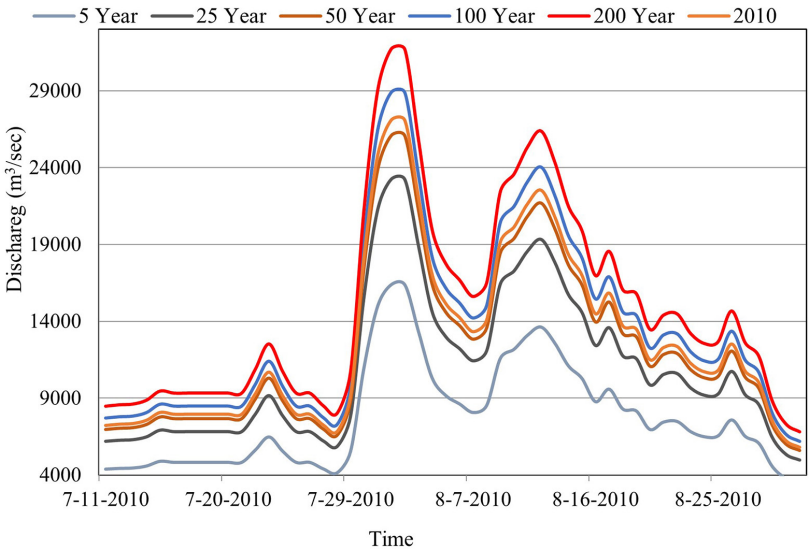

Figure 9. Discharge hydrographs for Chashma barrage at different return periods

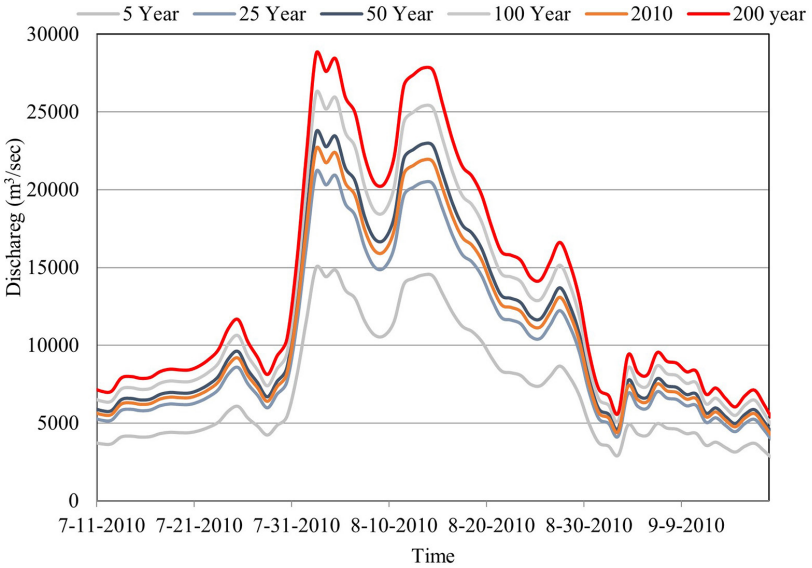

Figure 10. Discharge hydrographs for Taunsa barrage at different return periods

The optimized Manning's roughness coefficients of the main channel and floodplains were 0.027 and 0.055–0.040, respectively. The minor discrepancies in peak timing were due to unmodeled hill-torrent inflows, localized runoff, and infiltration. The observed and simulated Taunsa hydrographs for calibration and validation are compared in Figures 11 and 12, and the statistical performance metrics are presented in Table 3.

Extreme flood simulation and 200-year scenario analysis

HEC-RAS model calibration enabled the simulation of a 200-year return period flood with peak discharges of 31,728 and 28,723 m³/s at Chashma and Taunsa, respectively. When compared with the 2010 flood, areas which the flood simulation predicted would be inundated were much larger, at 3785 km² for the Chashma–Taunsa reach and 5101 km² for the Taunsa–Kot Mithon reach. MODIS imagery captured in 2010 shows an extent of 2995 km² of flooding in the Chashma–Taunsa reach, while the Taunsa–Kot Mithon reach shows an extent of 3030 km² (Figure 13). HEC-RAS simulation, on the other hand, estimated flooding extents of 3286 km² and 3185 km² for the respective reach, indicating a slight overestimation. Although the model produced 8.86% 4.87% overestimations in the Chashma–Taunsa and

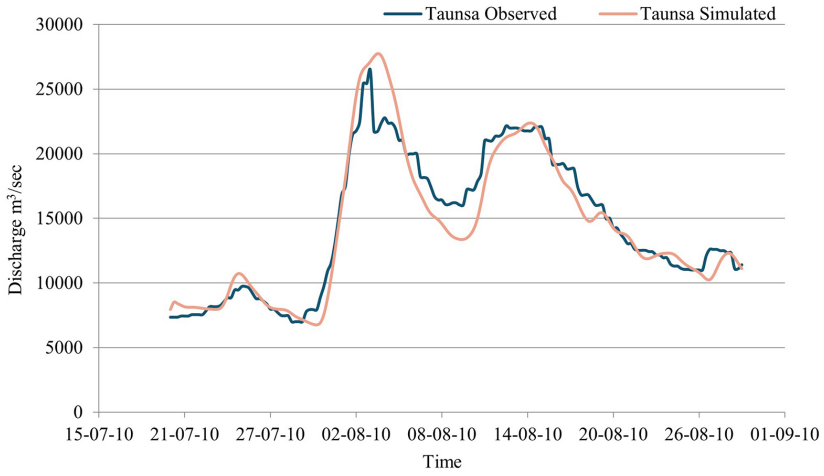

Figure 11. Observed vs. simulated hydrographs at Taunsa upstream for 2010 flood

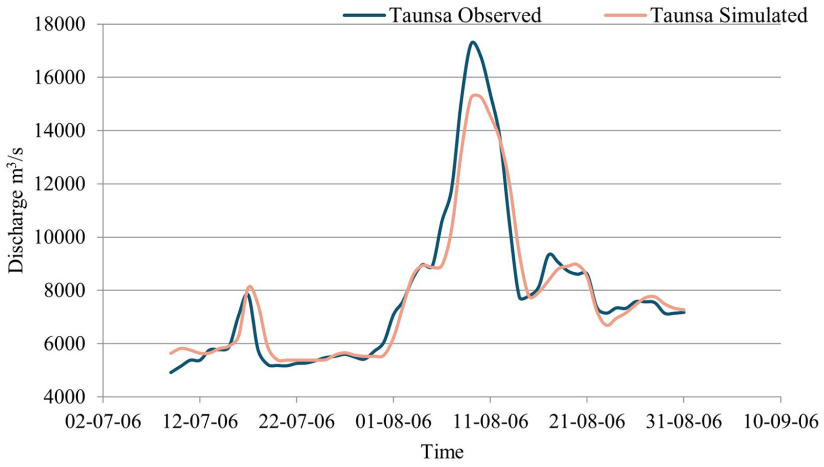

Figure 12. Observed vs. simulated hydrographs at Taunsa upstream for 2006 flood

Table 3. Calibration and validation using statistical performance metrics

Model performance parameter	Results of statistics					Model performance rank
	NSE	PBIAS %	RSR	R2	Correlation coefficient	
Calibration (2010 year)	0.92	2.07	0.28	0.91	0.95	Good
Validation (2006 year)	0.95	1.13	0.2	0.95	0.97	Good

Taunsa–Kot Mithon reaches, respectively, this confirms the model's reliability for simulating extreme flood scenarios and indicates its validation.

The model's 200-year scenario predicted a further 20.87% and 40.60% increase in inundated area over 2010 conditions for the Chashma–Taunsa and Taunsa–Kot Mithon reaches, respectively (Table 4). This finding suggests that the floodplains and floodplain wetlands adjacent to these river reaches exhibit profound differences in hydrologic response. This behavior, particularly the larger relative increase in Taunsa–Kot Mithon, suggests the possible predominance of Taunsa's floodplain in the hydrologic response of the entire reach. This suggests that floods have considerably large spatial variability.

To generate a continuous inundation profile across the Chashma–Kot Mithon corridor, flood maps for individual reaches were mosaicked and refined for city-scale analyses focusing on Layyah and Muzaffargarh, where Union Councils (UCs) were assessed under the 200-year scenario. As illustrated in Figure 14, flood depths across the study area ranged from 0 to 17 m, whereas flow

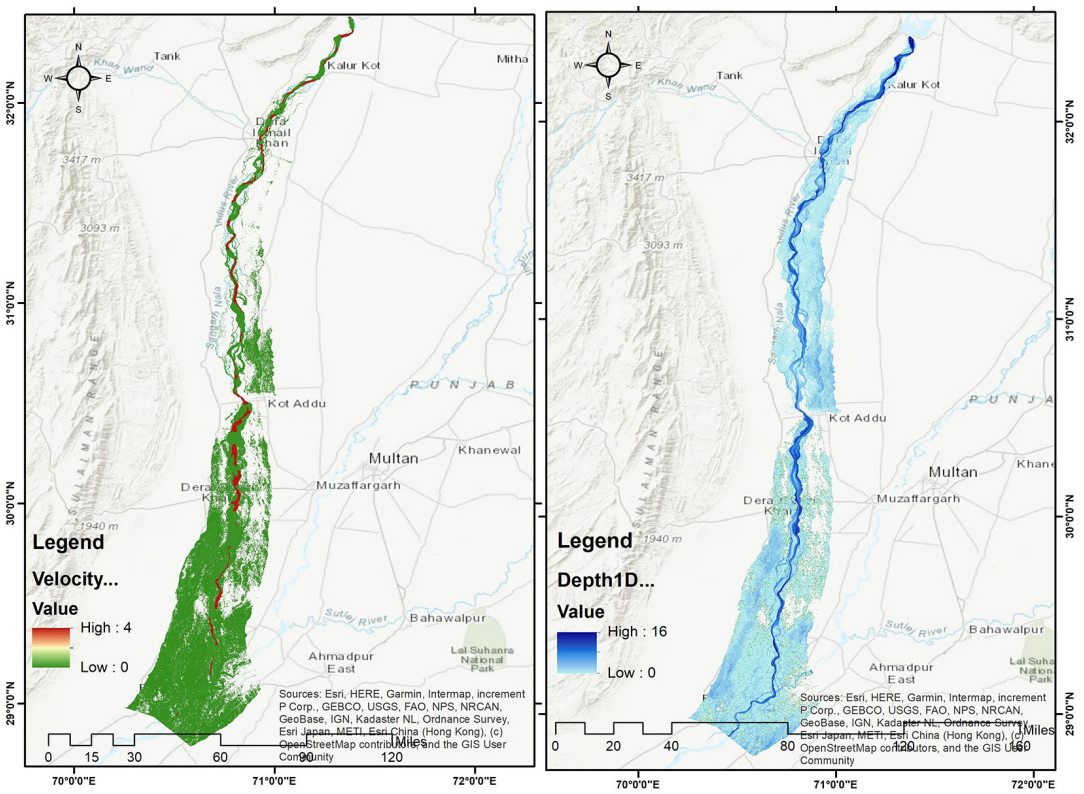

Figure 13. 2010-year flood at Chashma - Kot Mithon reach: (a) velocity map, (b) depth map

Table 4. Detailed comparison of the results

Parameter	Reach area (km²)	
	Chashma to Taunsa	Taunsa to Kot-Mithon
Modis area for 2010 flood	2995	3030
Model predicted area	3286	3185
Area under 200-year return period flood	3785	5101
Model predicted % more area vs Modis	8.86	4.87
% Area increase: 200-year return period flood vs. 2010 flood	20.87	40.6

velocities varied between 0 and 4 m/s, reflecting significant spatial heterogeneity in inundation extent, depth, and hydraulic intensity.

In the 2010 MODIS observation, Layyah and Muzaffargarh had 1276 km² and 1755 km² of flood area, respectively, which under the 200-year scenario, increased to 1420 km² (increased 10%) and 1968 km² (increased 11%), respectively (Table 5). In Muzaffargarh, the increased flood area remained larger; however, in both districts, the area of flooding was comparable in relative terms. This illustrates the extent of floodplain inundation during extreme events. Flood depth and velocity maps for Layyah and Muzaffargarh are presented in Figures 15 and 16, respectively, with the UC boundaries overlaid.

In Layyah, flood depths in low-lying depressions were greater than 11 m, and high-velocity flows (>2 m/s), which are indicative of severe erosion, were concentrated along active channels and breach paths. In the Muzaffargarh region, 15 m flood depths and 4 m/s flood velocities imposed severe conditions on socio-economically vulnerable and densely populated regions.

In the 200-year projection, several UCs are expected to submerge entirely. In Muzaffargarh, UCs Khangarh Doma, Langar Wah, Rampur, Bet Mir Hazar Khan, Beelay Wala, Bakaeni, Darain, Ghazi Ghat, Sheikh Umar, Bait Qaim Wala, and Hinjraee will be completely inundated, while Munhan, Budh, Wains, and Baz Wala will be partially submerged. In Layyah, full submergence

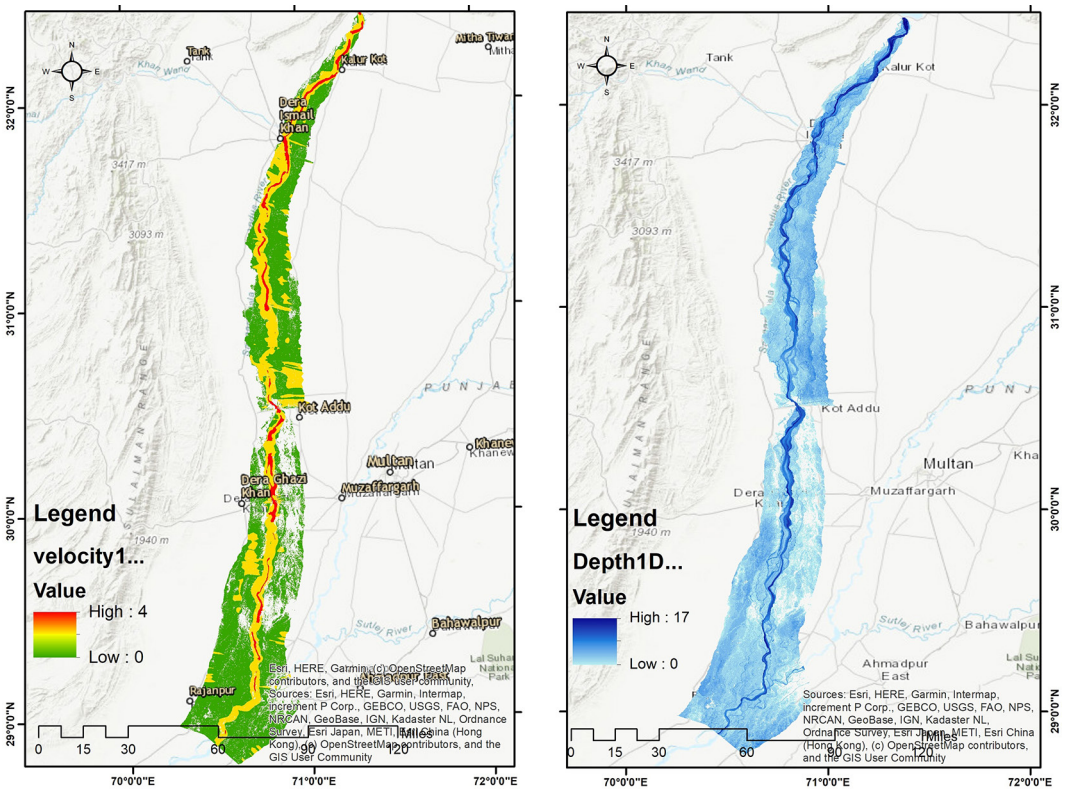

Figure 14. 200-year return period flood at Chashma – Kot Mithon: (a) velocity map, (b) depth map

Table 5. Detailed comparison of results for Layyah and Taunsa

City	Area under flood (km²)		% Increased flood area 200-YRP vs 2010
	2010-year flood	200-year flood	
Layyah	1276	1420	10
Muzaffargarh	1755	1968	11

is expected for Warah Serah, Basira, Basti Shadoo Khan, Kotla Haji Shah, Lohanch Nasheb, Jhakhar, Sarishtah, Bokhari Ahmed, And Bait Wasawa, while Sumita Karor Thal, Sanu Wala, Shah Pur, Jaman Shah, And Shumali Pahar Pur will be partially inundated.

Model evaluation and comparative context

The findings of this study reinforce the existing literature and strengthen the credibility of HEC-RAS–GIS integration for flood hazard assessment in Pakistan's river systems. Consistent with Ullah et al. (2024) and Khalil and Khan (2017), the application of the Generalized Extreme Value (GEV) distribution and its confirmed fit using Kolmogorov–Smirnov and Anderson–Darling tests aligns with best practices for estimating extreme discharges. The design discharge of 28,723 m³/s for the 200-year return period at Chashma closely matched the 29,897 m³/s reported by Khalil and Khan (2017), with differences attributable to the dataset coverage (2005–2022 versus 1971–2013).

Calibrated Manning's roughness coefficients 0.027 for the main channel, 0.055 for the left floodplain, and 0.044 for the right floodplain are consistent with values reported by Khalil and Khan (2017) and Afzal et al. (2022). The model performance indicators (R^2 = 0.91, RSR = 0.28, NSE = 0.92 for 2010 calibration; R^2 = 0.95, RSR = 0.20, NSE = 0.95 for 2006 validation) demonstrated strong inter- and intra-model agreement, exceeding most comparative studies in hydrodynamic modeling and validating the robustness of the methodology.

The inflow dataset was sufficient for validating the predictive capability because the simulated inundation extents closely matched the

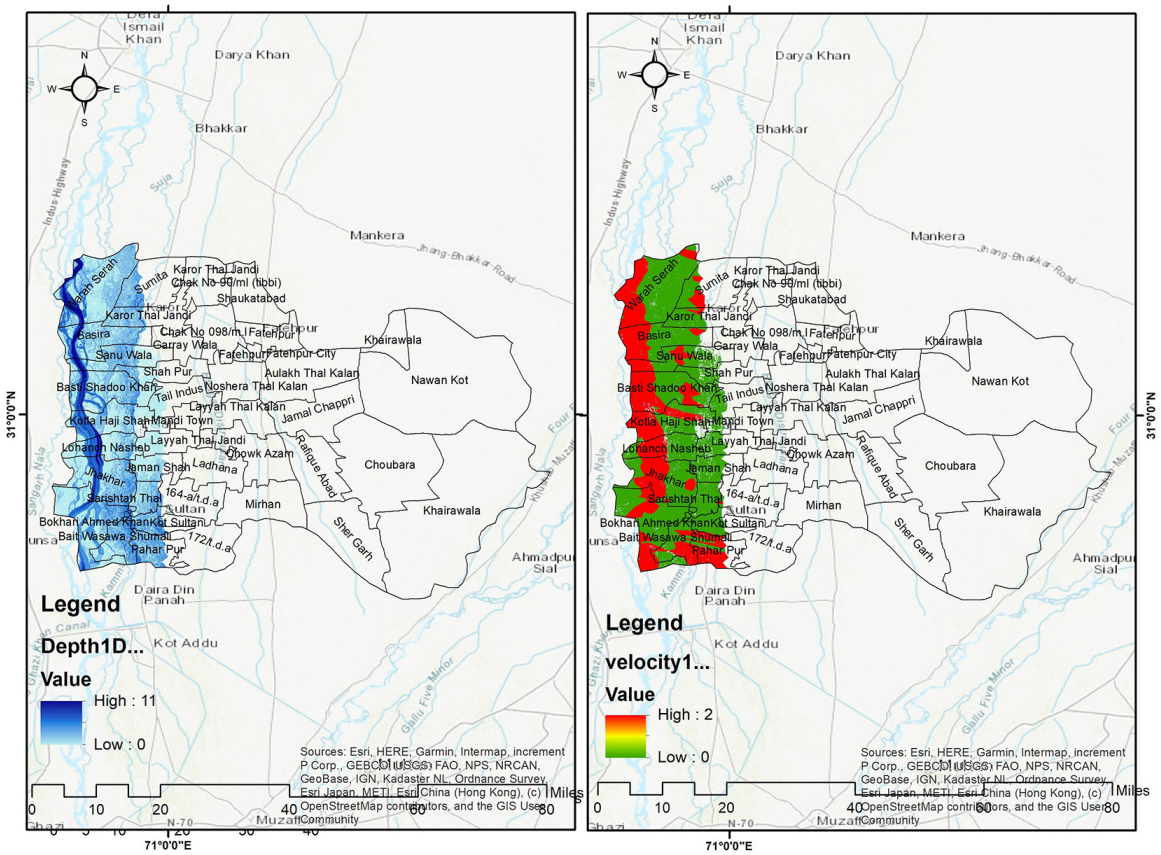

Figure 15. Layyah under 200-year return period flood: (a) depth map, (b) velocity Map

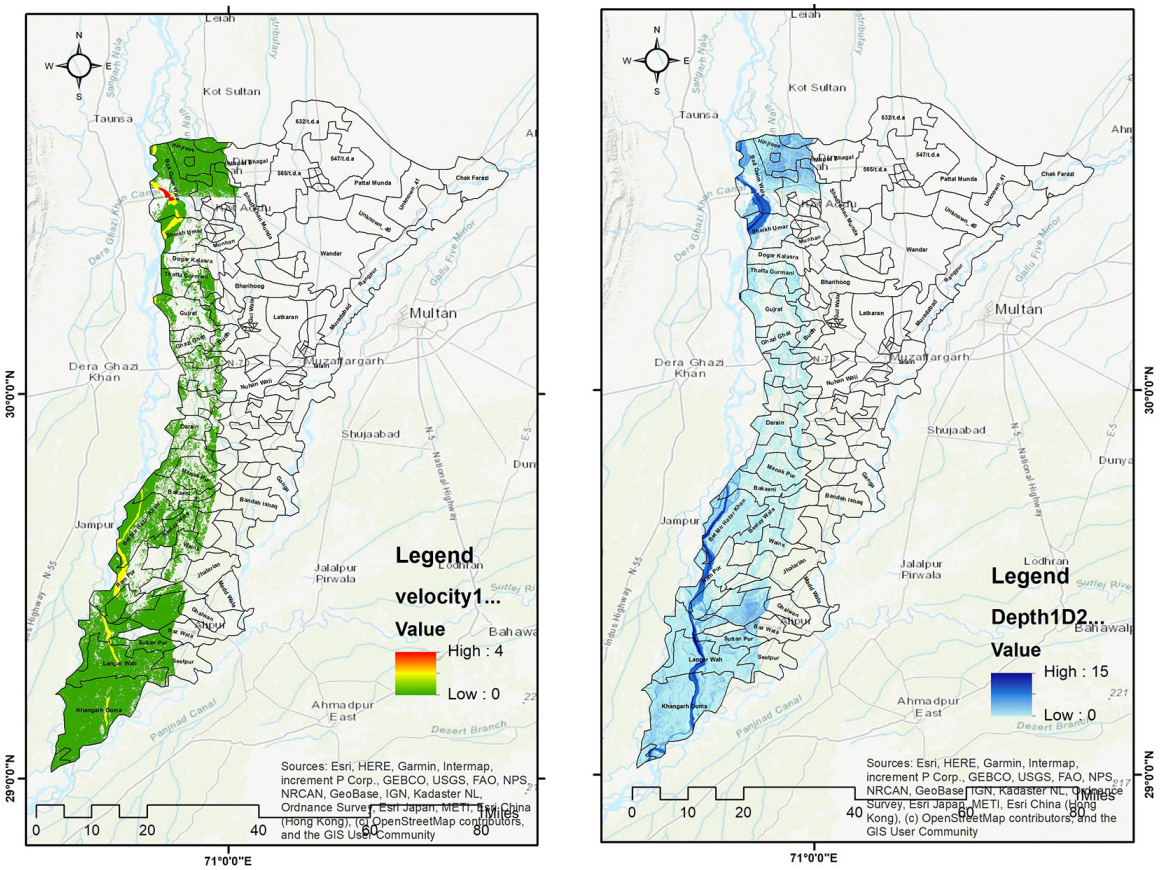

Figure 16. Muzaffargarh under 200-year return period flood: (a) velocity map, (b) depth map

MODIS-derived observations. Prior studies by Khattak et al. (2016) and Salman et al. (2021) highlighted terrain resolution and one-dimensional HEC-RAS modelling constraints; however, this study demonstrates that performance can be significantly improved through rigorous calibration, satellite-based validation, and statistical augmentation. The observed 40.6% increase in floodplain inundation under the 200-year scenario further supports characterizations by Khalil and Khan (2017) and Ullah et al. (2024) of the Indus floodplain's sensitivity to extreme discharges.

This integrated flood frequency and hydrodynamic analysis represents a comprehensive assessment of the extreme flood dynamics along the Chashma–Kot Mithon reach. By coupling statistical flood estimation with a rigorously calibrated and validated HEC-RAS model, this study achieved high-resolution predictions of inundation extent, depth, and flow velocity under both historical and extreme event scenarios. The application of robust external validation procedures and widely recognized performance metrics strengthens the reliability and credibility of these results. These findings establish a critical evidence base for data-driven flood risk management and resilience planning, addressing the urgent need within Pakistan's highly vulnerable riverine corridors.

CONCLUSIONS

Flooding in Pakistan's Indus River remains a persistent hydrological and socioeconomic challenge, yet district-scale hazard assessments are limited. This study addressed this gap by applying an integrated 1D HEC-RAS and GIS approach to the 432 km Chashma–Kot Mithon reach of the Indus River, Pakistan. Rigorous calibration and validation using hindcasting methods confirmed the model's reliability, with simulated inundation extents deviating by less than 9% from the MODIS observations.

Under the 200-year design flood scenario, peak discharges reached 31,728 m^3/s at Chashma and 28,723 m^3/s at Taunsa, inundating 3785 and 5101 km^2 in the respective reaches, representing increases of 20.9% and 40.6% over the 2010 superflood. Depth–velocity analysis revealed extreme hydraulic conditions, with depths of up to 17 m and velocities exceeding 4 m/s, particularly in Layyah and Muzaffargarh, where the flood hotspots expanded by up to 11%. Union Council–level overlays identified high-risk settlements concentrated along active flood corridors and in embankment failure zones.

The integration of HEC-RAS simulations with GIS-based hazard mapping provides a robust framework for flood risk assessment, emergency planning, and land-use regulation in the Indus Basin. Remote sensing data (MODIS and Landsat) were effective for parameter optimization and model validation. Future research should incorporate 2D hydraulic modeling, socioeconomic vulnerability assessments, and climate-driven hydrology forecasts to support comprehensive flood management strategies across Pakistan's river corridors.

Acknowledgment

The author gratefully acknowledges the Higher Education Commission (HEC) of Pakistan for support under the NRPU project (HEC/RandD/NRPU/2017/7431) and for awarding the International Research Support Initiative Program (IRSIP) scholarship, with special thanks to Prof. Dr. Venkatesh Merwade (Lyles School of Civil and Construction Engineering, Purdue University, USA) for guidance, and to Dr. Usman Khalil (AECOM, Australia), NESPAK, PMIU, and PID for their valuable data and assistance.

REFERENCES

1. Abbasnezhadi, K., Rousseau, A. N., Bohrn, S. (2020). Mid-21st century anthropogenic changes in extreme precipitation and snowpack projections over Newfoundland. *Canadian Water Resources Journal/Revue canadienne des ressources hydriques*, *45*(3), 216–236. https://doi.org/10.1080/07011784.2020.1760140
2. Abdrabo, K. I. A. (2023). Integrated urban hydrological approach for flood risk assessment and mitigation strategies in Egyptian cities. Kyoto University.
3. Afzal, M. A., Ali, S., Nazeer, A., Khan, M. I., Waqas, M. M., Aslam, R. A.,…Muzammil, M. (2022). Flood inundation modeling by integrating HEC–RAS and satellite imagery: a case study of the Indus River Basin. *Water*, *14*(19), 2984. https://doi.org/10.3390/w14192984
4. Ahmad, I., Wang, X., Waseem, M., Zaman, M., Aziz, F., Khan, R. Z. N., Ashraf, M. (2022). Flood management, characterization and vulnerability analysis using an integrated RS-GIS and 2D hydrodynamic

modelling approach: the case of Deg Nullah, Pakistan. *Remote Sensing*, *14*(9), 2138. https://doi.org/10.3390/rs14092138

5. Akhtar, M. (2023). Development of a web based GIS solution for flood inundation mapping and assessment in Lahore, Pakistan. *International Journal of Innovations in Science & Technology*, *5*(3), 298-307. https://doi.org/10.33411/IJIST/2023050201
6. Bajracharya, S. R., Shrestha, B. (2011). The status of glaciers in the Hindu Kush-Himalayan region. *International Centre for Integrated Mountain Development (ICIMOD)*. https://doi.org/10.53055/ICIMOD.551
7. Boucefiane, A., Meddi, M. (2022). Estimation of the probable maximum precipitation (PMP) in the Cheliff semi-arid region (Algeria). *Meteorology and Atmospheric Physics*, *134*(2), 34. https://doi.org/10.1007/s00703-022-00864-y
8. Brunner, G. W. (2010). HEC-RAS river analysis system: hydraulic reference manual.
9. Brunner, G. W. (2016). HEC-RAS River analysis system: hydraulic reference manual. Version 5.0. *US Army Corps of Engineers–Hydrologic Engineering Center*, *547*.
10. Cea, L., Costabile, P. (2022). Flood risk in urban areas: Modelling, management and adaptation to climate change. A review. *Hydrology*, *9*(3), 50. https://doi.org/10.3390/hydrology9030050
11. CEIWR-HEC. (2022). HEC-RAS Equations for Basic Profile Calculations. https://www.hec.usace.army.mil/confluence/rasdocs/ras1dtechref/6.3/theoretical-basis-for-one-dimensional-and-two-dimensional-hydrodynamic-calculations/1d-steady-flow-water-surface-profiles/equations-for-basic-profile-calculations
12. CEIWR-HEC. (2023). HEC-RAS Hydraulic Reference Manual. https://www.hec.usace.army.mil/confluence/rasdocs/ras1dtechref/6.3
13. CNN. (2010). Pakistan flood damage estimated at $9.7 billion. *Cable News Network*. http://www.cnn.com/2010/WORLD/asiapcf/10/14/pakistan.flood.cost/index.html
14. Coles, S., Bawa, J., Trenner, L., Dorazio, P. (2001). *An introduction to statistical modeling of extreme values* (Vol. 208). Springer.
15. Cook, A., Merwade, V. (2009). Effect of topographic data, geometric configuration and modeling approach on flood inundation mapping. *Journal of Hydrology*, *377*(1–2), 131–142. https://doi.org/10.1016/j.jhydrol.2009.08.015
16. Cui, T., Li, Y., Yang, L., Nan, Y., Li, K., Tudaji, M.,…Mubeen, A. (2023). Non-monotonic changes in Asian Water Towers' streamflow at increasing warming levels. *Nature Communications*, *14*(1), 1176. https://doi.org/10.1038/s41467-023-36804-6
17. FFC, F. (2010). Annual flood report 2018. Federal Flood Commission: Islamabad, Pakistan.
18. Floods, P. (2010). Preliminary damage and needs assessment. Asian Development Bank, Government of Pakistan, World Bank. Available at: http://reliefweb. int/sites/reliefweb. int/files/resources/64AE3DC5BEDA4E18492577DA001FBE55-Full_Report.pdf. Accessed: 12/24/2011.
19. George, S. L., Kantamaneni, K., V, R. A., Prasad, K. A., Shekhar, S., Panneer, S., Balasubramani, K. (2022). A multi-data geospatial approach for understanding flood risk in the coastal plains of Tamil Nadu, India. *Earth*, *3*(1), 383–400. https://doi.org/10.3390/earth3010023
20. Gomma, H. (2021). Floods hazards assessment by integrating hydrologic modeling and a geographic information systems (multi-criteria decision technique). *Journal of Al-Azhar University Engineering Sector*, *16*(61), 1007–1023. https://doi.org/10.21608/auej.2021.207517
21. Goodell, C. (2014). Breaking the Hec-Ras Code: A User's Guide to Automating Hec-Ras. H21s.
22. Gull, M., Khan, S., Nawaz, M., Hasan, M. U. (2020). Community based flood catastrophe preparedness, vulnerability, management and response of Layyah District, Punjab, Pakistan (1990–2015): Community Based Flood Catastrophe Preparedness, Vulnerability, Management and Response of Layyah District, Punjab, Pakistan (1990–2015). *International Journal of Economic and Environmental Geology*, *11*(2), 12-18.
23. Gumindoga, W., Liwonde, C., Rwasoka, D. T., Kowe, P., Maviza, A., Magidi, J.,…Tshitende, E. K. (2024). Urban flash floods modeling in Mzuzu City, Malawi Based on sentinel and MODIS data. *Frontiers in Climate*, *6*. https://doi.org/10.3389/fclim.2024.1284437
24. Hashmi, H. N., Siddiqui, Q. T. M., Ghumman, A. R., Kamal, M. A., Mughal, H. (2012). A critical analysis of 2010 floods in Pakistan. *African Journal of Agricultural Research*, *7*(7), 1054–1067.
25. Horritt, M., Bates, P. (2002). Evaluation of 1D and 2D numerical models for predicting river flood inundation. *Journal of Hydrology*, *268*(1–4), 87–99. https://doi.org/10.1016/S0022-1694(02)00121-X
26. Hosking, J. R. M., Wallis, J. R. (1997). *Regional frequency analysis*. Cambridge University Press.
27. Ibrahim, I., Ab Ghani, N., Asmawi, M. Z. (2024). Flood susceptibility assessment using multi-criteria analysis: Case Study in Selangor, Putrajaya, and Kuala Lumpur. *IOP Conference Series: Earth and Environmental Science*. https://doi.org/10.1088/1755-1315/1412/1/012009
28. Ijaz, S., Hameed, Q., Ahsan, A., Butt, M. A. (2019). Flood frequency analysis of Chenab River for predicting peak flows during late monsoon period. *Advances in Remote Sensing*, *8*(1), 1–29. https://doi.

org/10.4236/ars.2019.81001

29. Indrawati, D., Yakti, B. P., Purwanti, A., Hadinagoro, R. I. S. R. (2019). Computing urban flooding of meandering river using 2D numerical model (case study: Kebon Jati-Kalibata Segment, Ciliwung River Basin). *Matec Web of Conferences*, *270*, 04021. https://doi.org/10.1051/matecconf/201927004021
30. Khalil, U., Khan, N. M. (2017). Floodplain mapping for Indus river: Chashma–Taunsa reach. *Pakistan Journal of Engineering and Applied Sciences*.
31. Khan, H. U. A., Khalil, S. F. A., Kazmi, S. J. H., Umar, M., Shahzad, A., Farhan, S. B. (2017). Identification of river bank erosion and inundation hazard zones using geospatial techniques–a case study of Indus River Near Layyah District, Punjab, Pakistan. *Geoplan J Geomat Plan*, *4*, 121–130. https://doi.org/10.14710/geoplanning.4.2.121-130
32. Khan, M., Khan, A. U., Ullah, B., Khan, S. (2024). Developing a machine learning-based flood risk prediction model for the Indus Basin in Pakistan. *Water Practice & Technology*, *19*(6), 2213–2225. https://doi.org/10.2166/wpt.2024.151
33. Khattak, M. S., Anwar, F., Saeed, T. U., Sharif, M., Sheraz, K., Ahmed, A. (2016). Floodplain mapping using HEC-RAS and ArcGIS: a case study of Kabul River. *Arabian Journal for Science and Engineering*, *41*(4), 1375–1390. https://doi.org/10.1007/s13369-015-1915-3
34. Khosa, S. (2014). Re-Development, recovery and mitigation after the 2010 catastrophic floods: the Pakistani experience. In: Disaster and Development: Examining Global Issues and Cases (pp. 371-389). Springer. https://doi.org/10.1007/978-3-319-04468-2_21
35. Kim, V., Tantanee, S., Suparta, W. (2020). GIS-based flood hazard mapping using HEC-RAS model: a case study of lower Mekong River, Cambodia. *Geographia Technica*, *15*(1). https://doi.org/10.21163/gt_2020.151.02
36. Korjenić, A., Hrelja, E., Sivac, A., Banda, A. (2021). Application of GIS in the assessment of flood risk in the region Zenica-Doboj Canton. *Geographia Technica*, *16*. https://doi.org/10.21163/gt_2021.162.07
37. Lutz, A. F., ter Maat, H. W., Biemans, H., Shrestha, A. B., Wester, P., Immerzeel, W. W. (2016). Selecting representative climate models for climate change impact studies: an advanced envelope-based selection approach. *International Journal of Climatology*, *36*(12), 3988–4005. https://doi.org/10.1002/joc.4608
38. Manina, M., Halaj, P., Jurík, L., Kaletová, T. (2020). Modelling seasonal changes of longitudinal dispersion in the Okna river. *Acta Scientiarum Polonorum Formatio Circumiectus*, *19*(1), 37–46. http://doi.org/10.15576/ASP.FC/2020.19.1.37
39. Martin, M. (2023). The lifeblood of landscapes: understanding rivers and their vital role. *Journal of Environmental and Earth Science*, *7*(5), 1–5.
40. Moriasi, D. N., Arnold, J. G., Van Liew, M. W., Bingner, R. L., Harmel, R. D., Veith, T. L. (2007). Model evaluation guidelines for systematic quantification of accuracy in watershed simulations. *Transactions of the ASABE*, *50*(3), 885–900. https://doi.org/10.13031/2013.23153
41. Mujumdar, M., Bhaskar, P., Ramarao, M., Uppara, U., Goswami, M., Borgaonkar, H.,…Rajeevan, M. (2020). Droughts and floods. In: Assessment of climate change over the Indian region: a report of the Ministry of Earth Sciences (MoES), Government of India (pp. 117–141). Springer.
42. Nguyen, T.-H., El Outayek, S., Lim, S. H., Nguyen, V.-T.-V. (2017). A systematic approach to selecting the best probability models for annual maximum rainfalls – A case study using data in Ontario (Canada). *Journal of Hydrology*, *553*, 49–58. https://doi.org/10.1016/j.jhydrol.2017.07.052
43. OpenTopography. (2023). *Copernicus GLO-30 Digital Elevation Model*. https://portal.opentopography.org/raster?opentopoID=OTSDEM.032021.4326.3
44. Peker, İ. B., Gülbaz, S., Demir, V., Orhan, O., Beden, N. (2024). Integration of HEC-RAS and HEC-HMS with GIS in flood modeling and flood hazard mapping. *Sustainability*, *16*(3), 1226. https://doi.org/10.3390/su16031226
45. PMIU. (2022). *Programme Monitoring and Implementation Unit* https://irrigation.punjab.gov.pk/page/1086
46. Prasad, B., Rao, P. B., Ramamohanarao, P., Sarathkumar, S. (2022). Flood hazard vulnerability assessment by using geo spatial techniques: Krishna and Guntur Districts, Andhra Pradesh. *Current World Environment*, *17*(2), 498. https://doi.org/10.12944/cwe.17.2.20
47. Rizwan, M., Li, X., Chen, Y., Anjum, L., Hamid, S., Yamin, M., Shahid, M. A., Mehmood, Q. (2023). Simulating future flood risks under climate change in the source region of the Indus River. *Journal of Flood Risk Management*, *16*(1), e12857. https://doi.org/10.1111/jfr3.12857
48. Salman, A., Hassan, S. S., Khan, G. D., Goheer, M. A., Khan, A. A., Sheraz, K. (2021). HEC-RAS and GIS-based flood plain mapping: A case study of Narai Drain Peshawar. *Acta Geophysica*, *69*(4), 1383-1393. https://doi.org/10.1007/s11600-021-00615-4
49. Schürings, C., Feld, C. K., Kail, J., Hering, D. (2022). Effects of agricultural land use on river biota: a meta-analysis. *Environmental Sciences Europe*, *34*(1), 124. https://doi.org/10.1186/s12302-022-00706-z
50. Seyedeh, S., Thamer, A., Mahmud, A., Majid, K., Amir, S. (2008). Integrated modelling for flood hazard mapping using watershed modelling system. *Am. J. Eng. Appl. Sci*, *1*, 149–156. https://doi.org/10.3844/ajeassp.2008.149.156
51. Suro, T. P., Niemoczynski, M. J., Boetsma, A. (2024).

Development and calibration of HEC–RAS hydraulic, temperature, and nutrient models for the Mohawk River, New York. Scientific Investigations Report 2024-5005. https://doi.org/10.3133/sir20245005

52. Syvitski, J. P., Brakenridge, G. R. (2013). Causation and avoidance of catastrophic flooding along the Indus River, Pakistan. *GsA Today*, *23*(1), 4–10.
53. Tariq, A., Shu, H., Kuriqi, A., Siddiqui, S., Gagnon, A. S., Lu, L.,…Pham, Q. B. (2021). Characterization of the 2014 indus river flood using hydraulic simulations and satellite images. *Remote Sensing*, *13*(11), 2053. https://doi.org/10.3390/rs13112053
54. Teng, J., Jakeman, A. J., Vaze, J., Croke, B. F. W., Dutta, D., Kim, S. (2017). Flood inundation modelling: A review of methods, recent advances and uncertainty analysis. *Environmental Modelling & Software*, *90*, 201–216. https://doi.org/10.1016/j.envsoft.2017.01.006
55. Thaivalappil Sukumaran, S., Birkinshaw, S. J. (2024). Investigating the impact of recent and future urbanization on flooding in an Indian River catchment. *Sustainability*, *16*(13), 5652. https://doi.org/10.3390/su16135652
56. Ullah, M. I., Qureshi, K. S., Rauf, A. u., Shah, L. A. (2024). Advanced floodplain mapping: HEC-RAS and ArcGIS pro application on Swat River. *Journal of Umm Al-Qura University for Engineering and Architecture*, *15*(3), 245–258. https://doi.org/10.1007/s43995-024-00054-4
57. Velychko, S., Dupliak, O. (2024). Evaluation of the green flood mitigation measures in urban area in the frame of the sustainable city concept. *IOP Conference Series: Earth and Environmental Science.* https://doi.org/10.1088/1755-1315/1415/1/012008
58. Wang, X., Xie, H. (2018). A review on applications of remote sensing and geographic information systems (GIS) in water resources and flood risk management. *Water*, *10*(5), 608. https://doi.org/10.3390/w10050608
59. World Bank Group (2010). ADB-WB assess Pakistan flood damage at $9.7 billion. https://www.worldbank.org/en/news/press-release/2010/10/14/adb-wb-assess-pakistan-flood-damage-at-97-billion
60. Yonehara, S., Kawasaki, A. (2020). Assessment of the tidal effect on flood inundation in a low-lying river basin under composite future scenarios. *Journal of Flood Risk Management*, *13*(3), e312606. https://doi.org/10.1111/jfr3.12606
61. Younas, A., Khan, A., Abubakar, H. M., Tahseen, Z., Arshad, A., Taj, M., Nazir, U. (2024). 2022 Flood impact in Pakistan: Remote sensing assessment of agricultural and urban damage. arXiv:2410.07126. https://doi.org/10.48550/arXiv.2410.07126